




RESEARCH ARTICLE

10.1002/2016JC012353

Observed cold filaments associated with mesoscale eddies in the South China Sea

Jiaxun Li¹ , Guihua Wang^{1,2} , and Xiaoming Zhai³ 

Key Points:

- First reporting of the fascinating cold filaments in the spring intermonsoon in the South China Sea
- The formation and variability of the cold filaments are associated with mesoscale eddies
- Profound effects of the cold filaments on the chlorophyll a concentration and the overlying atmosphere

Correspondence to:

G. Wang,
wghocean@yahoo.com

Citation:

Li, J., G. Wang, and X. Zhai (2017), Observed cold filaments associated with mesoscale eddies in the South China Sea, *J. Geophys. Res. Oceans*, 122, 762–770, doi:10.1002/2016JC012353.

Received 18 SEP 2016

Accepted 5 JAN 2017

Accepted article online 10 JAN 2017

Published online 31 JAN 2017

Corrected 6 APR 2017

This article was corrected on 6 APR 2017. See the end of the full text for details.

¹Institute of Atmospheric Science, Department of Environmental Science and Engineering, Fudan University, Shanghai, China, ²State Key Laboratory of Satellite Ocean Environment Dynamics, Second Institute of Oceanography, State Oceanic Administration, Hangzhou, China, ³Centre for Ocean and Atmospheric Sciences, School of Environmental Sciences, University of East Anglia, Norwich, United Kingdom

Abstract Unusual cold filaments are uncovered during the spring intermonsoon season in the South China Sea (SCS) using a suite of satellite observations. They have a width of about 100 km on average and extend several hundreds of kilometers offshore on the sea surface, providing significant cross-shelf transport of heat and nutrients. The eastward current associated with mesoscale eddies in spring in the western SCS found to play an important role in the filament formation by advecting coastal cold waters far offshore. The meridional location of the cold filament displays considerable interannual variability ranging between 9°N and 18°N, which can be attributed to the interannual south-north shift of the eastward current associated with eddies. It is also found that in the spring, cold filaments have profound effects on the chlorophyll a concentration in the upper ocean as well as the overlying atmosphere. These findings provide new insights into the role of eddies in cross-shelf exchange and mesoscale air-sea interaction in the marginal seas.

1. Introduction

The robust feature of cold filaments, previously also referred to as cold tongues, plumes, or squirts, is that cold water may extend hundreds of kilometers in narrow bands [Flament *et al.*, 1985]. Cold filaments are often associated with strong offshore currents, and found to make a significant contribution to the material exchange between the nutrient-rich coastal water and the oligotrophic open ocean [Washburn *et al.*, 1993]. Cold filaments are frequently seen in the California Current System [Mooers and Robinson, 1984; Strub *et al.*, 1991], off the coast of Iberia [Barton *et al.*, 2001; Peliz *et al.*, 2004; Meunier *et al.*, 2012], and in the southeast Atlantic Ocean [Lutjeharms *et al.*, 1991].

The South China Sea (SCS) is a semienclosed sea subject to the dramatic seasonal variation of the East Asian Monsoon. In winter, the wind forcing over the SCS is dominated by the strong prevailing northeasterly monsoon, while in summer the winds reverse direction to southwesterly [e.g., Liu and Xie, 1999]. Spring and autumn are transition seasons in which winds switch from northeasterly to southwesterly and southwesterly to northeasterly, respectively. Cold filaments have been found in the SCS in summer arising from the eastward ocean current associated with the southwest wind jet [Xie *et al.*, 2003, 2007; Chen and Wang, 2014]. However, a question remains as to whether cold filaments can exist in the other seasons?

Using a suite of high resolution satellite products, we found a set of fascinating beard-like cold filaments off the western coastal boundary of the SCS in the spring intermonsoonal season (April and May), which are somewhat different from the current-jet driven summer cold filaments. The cold filaments during the spring intermonsoon are much narrower and weaker than those in summer. A snapshot of sea surface temperature (SST) on 17 May 2005 shows three cold filaments: one cold filament starts at around 14°N, 109°E, and extends eastward all the way to 15°N, 112.2°E (Figure 1a), and the other two cold filaments occur at around 16°N and 12.5°N, respectively. Corroborating evidence for the existence of the three cold filaments is found in satellite ocean color observations (Figure 1b), which reveal three colocated tongue-shaped, high-chlorophyll a (*Chl a*) concentration blooms. These filaments are fascinating and quite beautiful in their complexity. Although some cases of high *Chl a*

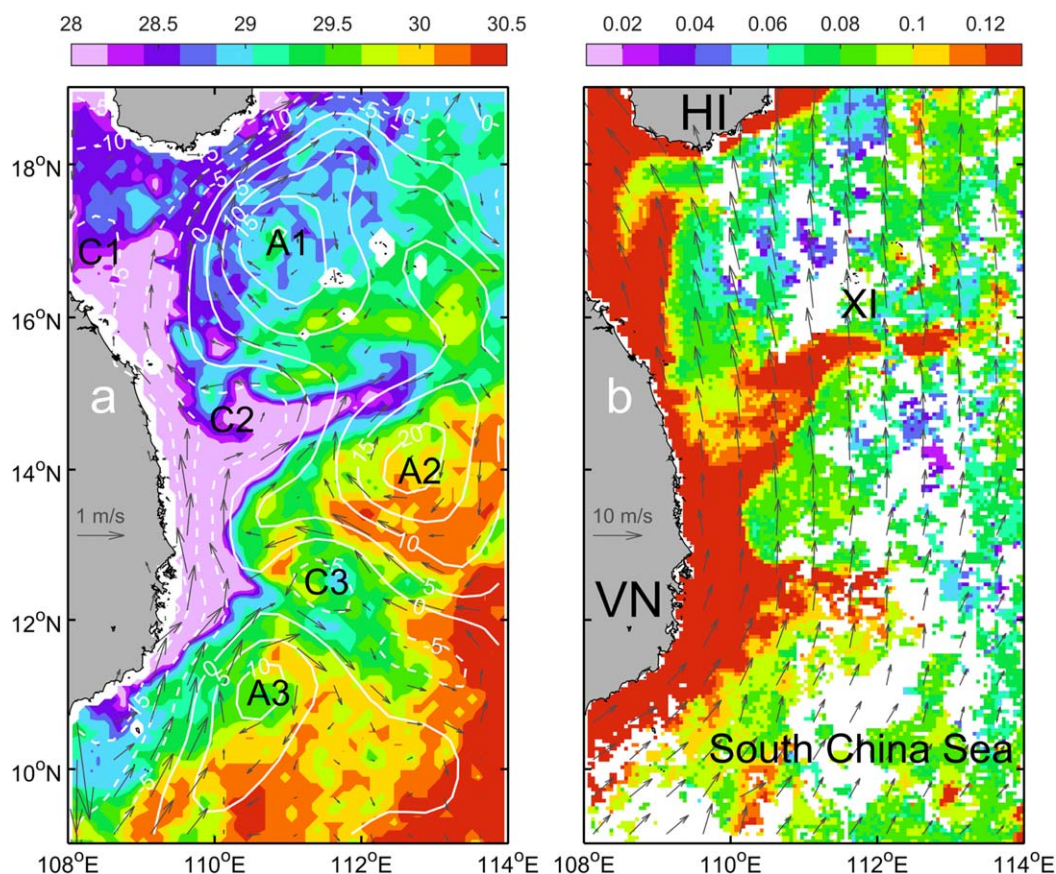


Figure 1. Snapshot of (a) RSS SST (color, °C), SLA (contours at 5 cm intervals), geostrophic current anomalies (gray vectors). The three anticyclonic (cyclonic) eddies are labeled as A1 (C1), A2 (C2), and A3 (C3). (b) MODIS Aqua sea surface *Chl a* concentration (color, mg m^{-3}) and sea surface wind vectors on 17 May 2005. In Figure 1b, HI: Hainan Island, XI: Xisha Islands, and VN: Vietnam.

concentration in narrow bands were found in the SCS during the spring intermonsoon season before [Lin *et al.*, 2010; Wang and Tang, 2014], there have been no prior reports on the SST signal and no systematic investigations on these filaments. In this paper, we will statistically analyze the spatial and temporal features of these unusual spring cold filaments, then explore their underlying formation mechanisms, and finally discuss their impacts on the atmosphere.

2. Data and Methods

2.1. Data

Multiple sets of satellite data are used, including: (1) the Remote Sensing Systems (RSS, ftp://data.remss.com/SST/daily_v04.0/mw_ir/) SST daily product with 9 km resolution for the period from 1 January 2003 to 31 December 2013; (2) the MODerate resolution Imaging Spectroradiometer (MODIS, <http://oceancolor.gsfc.nasa.gov/>) Aqua 8 day sea surface *Chl a* concentration with 4 km resolution from January 2003 to May 2015; (3) the Quick Scatterometer (QuikSCAT, <http://data.remss.com/qscat/>) and the Advanced SCATterometer (ASCAT, <ftp://ftp.remss.com/ascat/>) daily wind data with 0.25° grid for the period from 1 January 2003 to 31 December 2013; (4) the Archiving, Validation and Interpretation of Satellite Oceanographic data (AVISO, <ftp://ftp.aviso.oceanobs.com/>) daily sea level anomalies (SLA) data with 0.25° grid from 1 January 2003 to 31 December 2013 [Ducret *et al.*, 2000].

The SCS eddy trajectory data are derived from the third release global eddy data set (<http://cioss.coas.oregonstate.edu/eddies/>). However, only eddies with lifetimes of 4 weeks or longer are retained in this data set. The eddy positions within their trajectories are recorded at 7 day time intervals. A detailed description of the eddy trajectory data set can be found in Chelton *et al.* [2011].

2.2. Model

A simple mixed layer model [Qu, 2001] is used to investigate the formation mechanisms of the cold filaments. The model is based on the mixed layer temperature equation [Wang *et al.*, 2012; Sun *et al.*, 2016], except that only the geostrophic component of the advection of mixed layer temperature is included. Consequently, the equation for the mixed layer temperature tendency is

$$\frac{\partial T}{\partial t} = - \left(u_g \frac{\partial T}{\partial x} + v_g \frac{\partial T}{\partial y} \right)$$

where T is the SST or the mixed layer temperature, t is time; x and y are the conventional Cartesian coordinates, u_g and v_g are the geostrophic components of ocean velocity in x and y directions, respectively. The temperature field is initialized with the RSS SST in April averaged from 2003 to 2013, which is linearly interpolated onto the grids of AVISO geostrophic currents. The horizontal resolution of the model is $1/4^\circ$, and the time step is 1 h. The model is assumed to reach equilibrium once the temperature difference between two successive time steps is less than 0.1°C . In this simple model, air-sea heat exchanges, entrainment at the base of the mixed layer and horizontal mixing with the surrounding water are not considered.

2.3. Filament Detection

The methodology used for SST or *Chl a* concentration filament identification is similar to the procedure described by Haynes *et al.* [1993] and Cordeiro *et al.* [2015], which mainly consists of two procedures: first, the pixels with an SST (*Chl a*) meridional gradient higher than $0.03^\circ\text{C}/\text{km}$ ($0.001 \text{ mg m}^{-3}/\text{km}$) are marked on each SST (*Chl a*) image, in order to highlight frontal regions. It should be noted that the threshold of $0.03^\circ\text{C}/\text{km}$ ($0.001 \text{ mg m}^{-3}/\text{km}$) was reached empirically. Higher threshold values than the currently chosen ones may overlook some weak filaments. Second, according to the definition of filament, the southern and northern boundaries of the filament can be marked and the mid-latitudes between the two boundaries were recorded in each 0.25° grid along the filament. Only the filaments originating from the western coast of the SCS were taken into account in this study.

3. Results

3.1. Observation of the Cold Filaments

To understand the general features of the springtime cold filaments, Figure 2a shows the cold filaments identified from the daily RSS SST images during April and May. This period is during the SCS monsoon transition time from winter northeasterly winds to summer southwesterly winds. The statistical analysis is over the years 2003 to 2013. The cold filaments are observed on a total of 229 days, which is roughly 34.1% of the total days of the spring intermonsoon period. The cold filaments occur between 10°N and 17°N , and extend several hundreds of kilometers from the western coastal boundary to the open ocean. The cold filaments are usually accompanied by high *Chl a* concentration phytoplankton blooms. The filaments derived from the high *Chl a* concentration zone also appear in similar regions (Figure 2b), which suggests that there may be a more general relationship between changes of SST and *Chl a* in the filament regions. The spatial correlation between SST and *Chl a* concentration in cold filament bands is relatively high with $R^2 = 0.33$ (Figure 3a). Note that the number of *Chl a* blooms from MODIS Aqua (64) is significantly less than that from RSS SST (229) because the temporal resolution for MODIS is 8 days, while that for RSS is 1 day and the satellite images of *Chl a* blooms are sometimes contaminated/missing due to cloud cover. Due to the discrepancy of time resolution among *Chl a* (8 days), SST (daily), and wind (daily), the set of locations on *Chl a* filaments from 2003 to 2013 was used as the filament regions, and the SST and wind speed data on the same day were linearly interpolated into the *Chl a* filament locations for consistency.

Table 1 lists the occurrence date, occurrence frequency, number, length, and strength of the SST cold filaments observed for each year. These results show that the filaments demonstrate significant year to year variability. Filaments are typically located between 12°N and 16°N in most years; however, it is important to note that the locations of cold filaments sometimes display significant meridional shifts. For example, some filaments in 2003 and 2008 occurred north of 16°N , while in 2004 filaments appeared south of 12°N . These three geographical zones can also be clearly seen from Figure 4a: the filaments occur most around the three latitude bands: $16\text{--}18^\circ\text{N}$, $12\text{--}16^\circ\text{N}$, and $10\text{--}12^\circ\text{N}$, with peak values centered at 17.6°N , 14.8°N , and 10.5°N ,

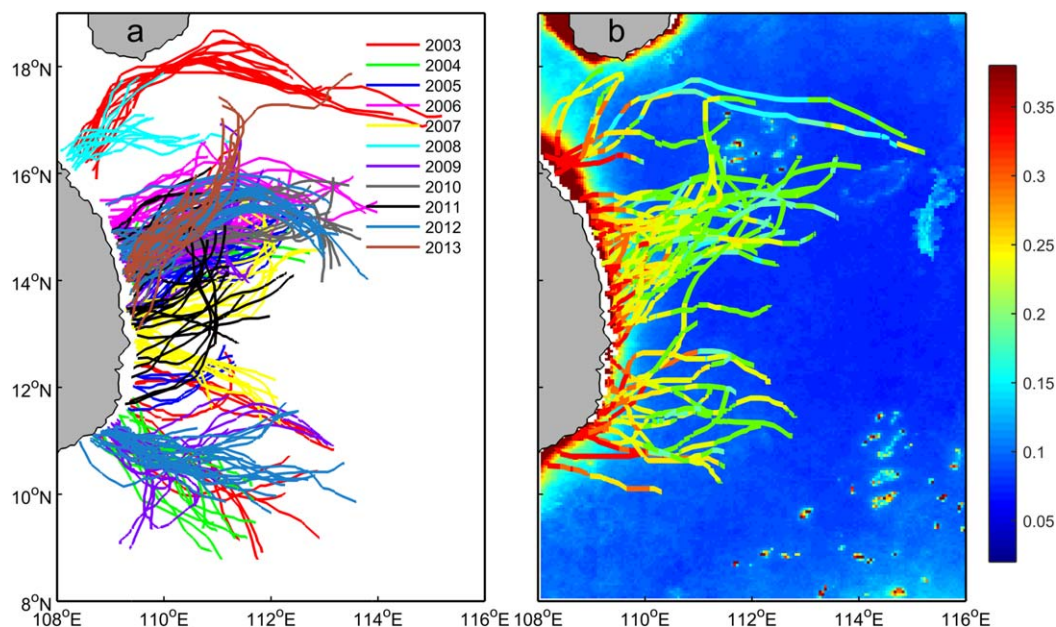


Figure 2. (a) Distribution of springtime cold filaments in the western SCS for 2003–2013 derived from the daily RSS SST images. (b) Distribution of phytoplankton blooms derived from the MODIS Aqua 8 day sea surface *Chl a* concentration images. In Figure 2b, the colorful ribbons represent the values of *Chl a* concentration in phytoplankton blooms relative to the spring climatology of *Chl a* concentration shown by the background color.

respectively. Consequently, we classify these filaments into three types from north to south: northward shifted, normal, and southward shifted, respectively.

We make several composite images based on the filament types. For the northward (southward) shifted type, we select all the cold filaments cases in the spring of 2008 (2004) (Figures 5a and 5c). The locations of the cold filaments for these two types and their corresponding SLA maps are quite different from the normal type, for which we use the composites in 2007 as typical (Figure 5b). For the northward (southward) shifted type, the cold filament moves about 3° northward (2° southward) from the location of the normal type. It should be noted that two or all three types of cold filaments can occur in a single year. For example, two cold filaments appear simultaneously around 14.5°N and 11°N in the composite map in 2012. These intriguing filaments appear in the SCS in the spring intermonsoon season with very different characteristics from those found in summer, when only a strong and wide filament appears in a single year.

3.2. Dynamic Linkage Between Cold Filaments and Eddies

To investigate the dynamics of cold filament formation in the spring intermonsoon season, we examined daily images of SST, SLA, and sea surface winds. The snapshot on 17 May 2005 (Figure 1a) suggests that cold filaments in the western SCS could be associated with the eastward currents on the joint flank between

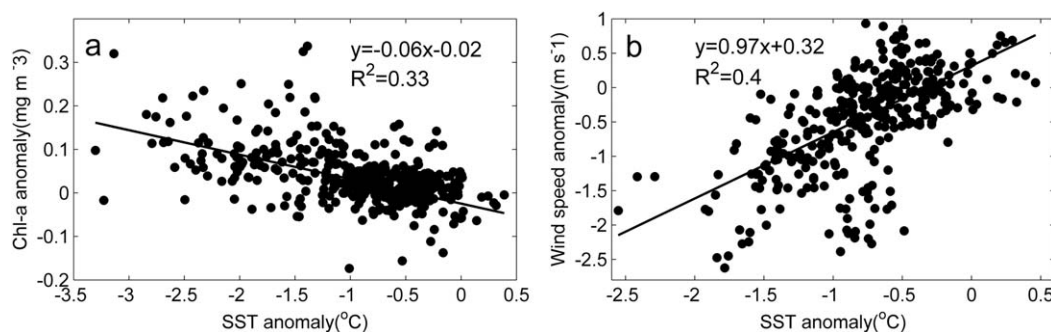


Figure 3. Scatterplots of (a) SST anomalies versus *Chl a* concentration anomalies with best fit linear regression and (b) SST anomalies versus wind speed anomalies with best fit linear regression in the regions of the *Chl a* filaments from 2003 to 2013.

Table 1. Statistics of the Cold Filaments Identified in the Western SCS in April and May From 2003 to 2013 Based on the Daily RSS SST Images

Year	2003	2004	2005	2006	2007	2008	2009	2010	2011	2012	2013
No.	30	26	31	42	22	13	32	26	22	41	16
P	49.2%	42.6%	50.8%	68.9%	36.1%	21.3%	52.5%	42.6%	36.1%	67.2%	26.2%
T _{first}	04–08	04–14	04–22	04–01	04–19	04–04	04–16	05–06	04–27	04–27	05–15
T _{last}	05–31	05–29	05–20	05–12	05–30	04–16	05–30	05–31	05–28	05–31	05–30
<L>	486.2	285.4	286.0	338.4	347.6	234.0	332.0	362.7	280.0	420.1	358.7
Max(L)	844.6	403.1	431.4	593.5	590.5	386.5	604.8	618.8	501.6	599.4	698.2
Min(L)	160.8	132.6	180.2	126.2	207.8	158.7	157.1	92.5	113.5	234.1	207.3
<S>	0.88	1.12	0.88	0.51	0.42	0.41	0.36	0.63	0.53	0.68	0.73
Max(S)	1.52	1.96	1.84	1.22	0.87	1.01	1.31	1.48	0.86	1.72	1.18
Min(S)	0.06	0.44	0.14	0.08	0.10	0.01	0.02	0.02	0.23	0.01	0.28

^aNote: No.: number of cold filaments; P: occurrence possibility; T_{first}: date of the first appearance; T_{last}: date of the last appearance; L: length of the filament (defined as the curving line distance between a filament's initial and end positions, in km); S: strength of the filament (defined as the SST difference between a filament and its climatology, in °C); < >: average of the group.

an anticyclonic eddy and a cyclonic eddy, northern flank of an anticyclonic eddy, or southern flank of a cyclonic eddy. Figures 5a–5d show the composites for 2008, 2007, 2004, and 2012, corresponding to northward shifted, normal, southward shifted, and mixed type filaments, respectively. All of them demonstrate that an eastward current associated with eddies always exists where there is a cold filament, strongly suggesting that the eastward current in the western SCS may have an important role to play for the formation of cold filaments.

To verify this hypothesis, we followed the life cycle of cold filaments from 21 April 2006 to 12 May 2006. Figure 6a shows the time-latitude evolution of the SST anomalies and the zonal geostrophic velocity anomalies at 109.5°E for this time period. As can be seen, there is a strong eastward current with a magnitude of

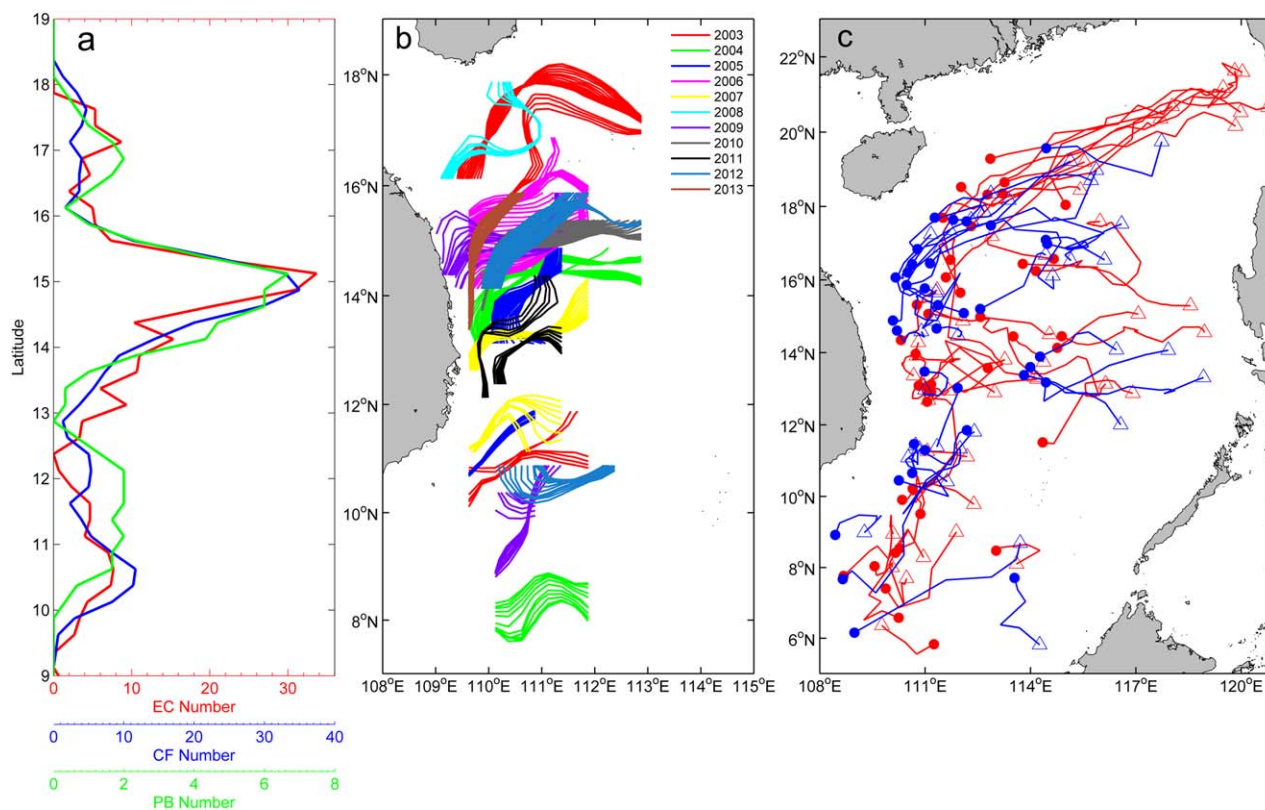


Figure 4. (a) Number distributions of the eastward currents (EC, red line), cold filaments (CF, blue line), and phytoplankton blooms (PB, green line) for each 0.25 degree latitude bin (zonally averaged) after 3-points smoothing; (b) locations of the springtime eastward currents in the western SCS from 2003 to 2013; (c) tracks of the anticyclonic eddies (red line) and cyclonic eddies (blue line) in spring. The empty triangle (solid circle) represents the starting (ending) position of each eddy track.

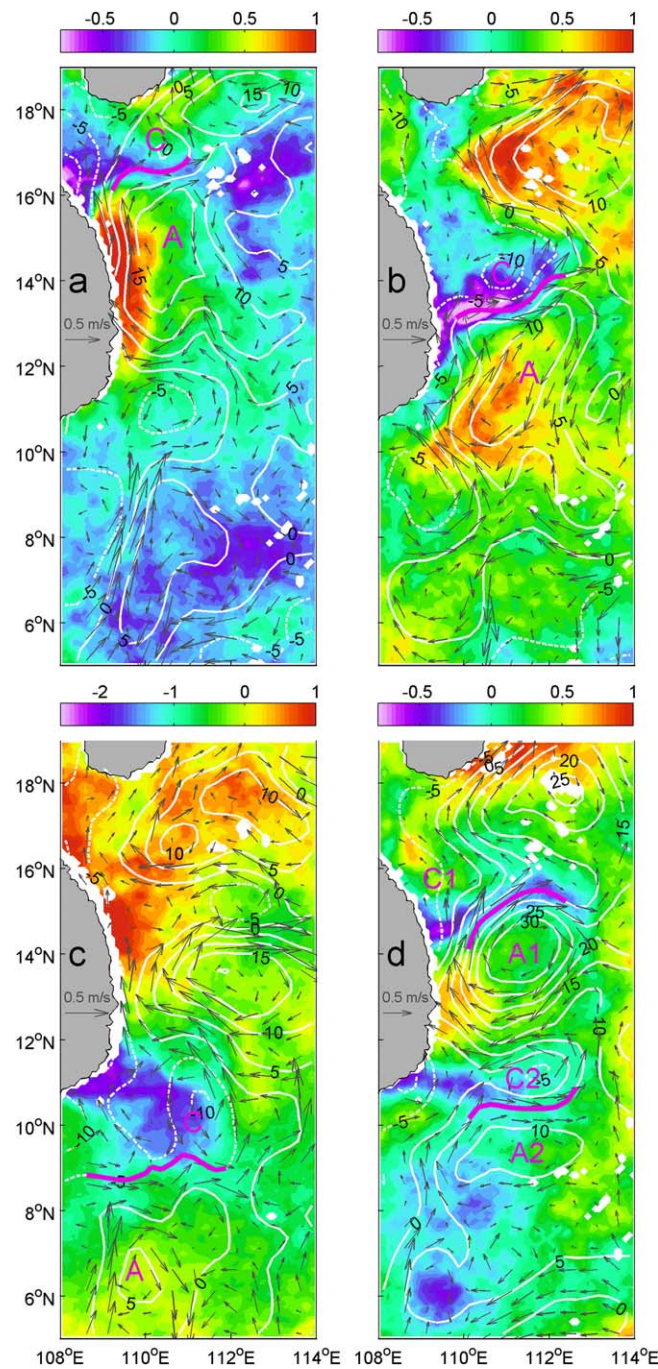


Figure 5. Composites of RSS SST anomalies ($^{\circ}\text{C}$, color shading) and SLA (contours at 5 cm intervals) in (a) 2008, (b) 2007, (c) 2004, and (d) 2012 representing the four cases: northward shifted type, normal type, southward shifted type, and mixed type, respectively. Pink thick lines are for the locations of the eastward currents. Anticyclonic (cyclonic) eddies are labeled with A (C).

ward currents versus latitude peaks at three latitudes: 17.2°N, 15.2°N, and 10.7°N (Figure 4a). The spatial distribution of the eastward currents is quite similar to the cold filaments discussed above. The above analysis suggests that there is a close dynamic linkage between the north-south shift of cold filaments and the eastward currents in the western SCS in the spring intermonsoon season. As the eastward current moves northward (southward), the center of the cold filament on its main stream is displaced northward (southward) along with it.

~30 cm/s in the core of cold filaments. In the spring intermonsoon season in the western SCS, these strong eastward currents tend to be associated with the dipole (an anticyclonic eddy to the south and a cyclonic eddy to the north) and occur between the two eddies (e.g., Figure 1a). To confirm the role of the eastward current in the cold filament formation, we apply the mixed layer model described in section 2.2 which includes only geostrophic advection. Figure 7b shows that the cold filament can be reproduced reasonably well by the simple mixed layer model, although the simulated cold filament is somewhat wider than the satellite observation (Figure 7c) due to the coarse resolution of the AVISO SLA data. The statistical relationship and the model result both suggest that geostrophic advection by the eastward current associated with eddies plays an important role in the cold filaments formation.

To investigate the causes of the meridional shifts of the cold filaments, we calculate the average locations of cold filaments and the associated eastward currents in each year from 2003 to 2013 (Figure 8). It is noted that the zero vorticity contour of the dipole is used to present the core location of the eastward current [Chen and Wang, 2014]. The correlation between the average locations of cold filaments and the associated eastward currents reaches 0.84, which is significant at the 95% confidence level. This strong correlation suggests that the cold filaments are tied to the meridional shift of the eastward currents and associated eddies on interannual time scales. We further identify all the eastward currents associated with cold filaments from satellite altimeter data (Figure 4b). The number distribution of eastward currents versus latitude peaks at three latitudes: 17.2°N, 15.2°N, and 10.7°N (Figure 4a). The spatial distribution of the eastward currents is quite similar to the cold filaments discussed above. The above analysis suggests that there is a close dynamic linkage between the north-south shift of cold filaments and the eastward currents in the western SCS in the spring intermonsoon season. As the eastward current moves northward (southward), the center of the cold filament on its main stream is displaced northward (southward) along with it.

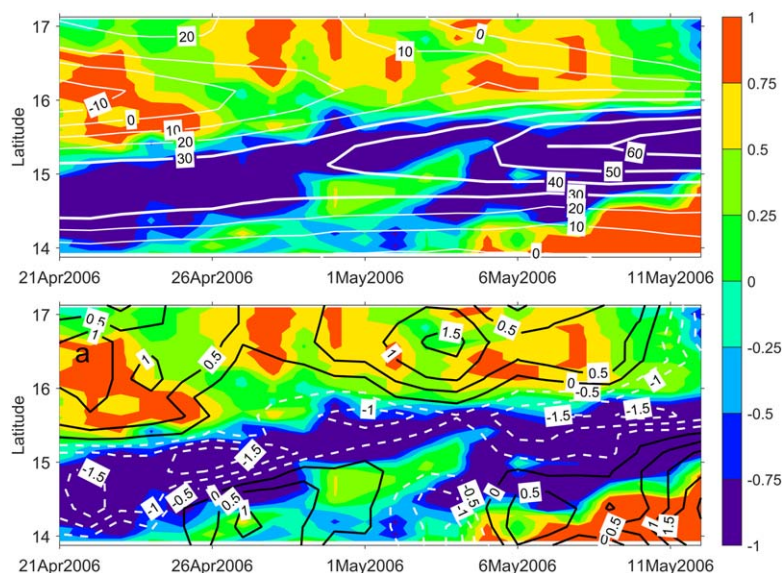


Figure 6. Time-latitude diagrams of (a) zonal geostrophic current velocity anomalies (cm/s, contour) and SST anomalies (°C, color shading) with the meridional mean removed, and (b) wind speed anomalies (m/s, contour) and SST anomalies (°C, color shading) with the meridional mean removed from 21 April 2006 to 12 May 2006 at 109.5°E.

Moreover, by monitoring the tracks of the spring anticyclonic and cyclonic eddies in the western SCS from the satellite altimeter data (Figure 4c), we found that there are different sources of these eddies for each geographic zone. In the more northern latitudes (16–20°N), the anticyclonic eddies in the western SCS can be traced back to the southwest of Taiwan Island. After their generation in winter, they propagate southwestward until reaching the vicinity of Xisha Island (16.5°N, 112°E). As for the cyclonic eddies in the more northern latitudes, they are either generated locally or come from the central SCS. In the central latitudes (12–16°N), the anticyclonic and cyclonic eddies are either generated locally or come from a region to the west of Luzon Island in winter. In the more southern latitudes (5–12°N), most of the anticyclonic and cyclonic eddies are locally generated in the western SCS and propagate relatively short distances. Although the mechanisms of eddy generation and filament formation need to be further verified, the geographic relationship between the eddy distributions and the typical locations of cold filaments suggests that the eastward current associated with eddies is responsible for the cold filament formation in the western SCS in the spring intermonsoon season.

4. Summary and Discussion

The spatial distribution and interannual variability of cold filaments in the western SCS formed during the intermonsoon season are presented and discussed for the first time using a suite of satellite observations.

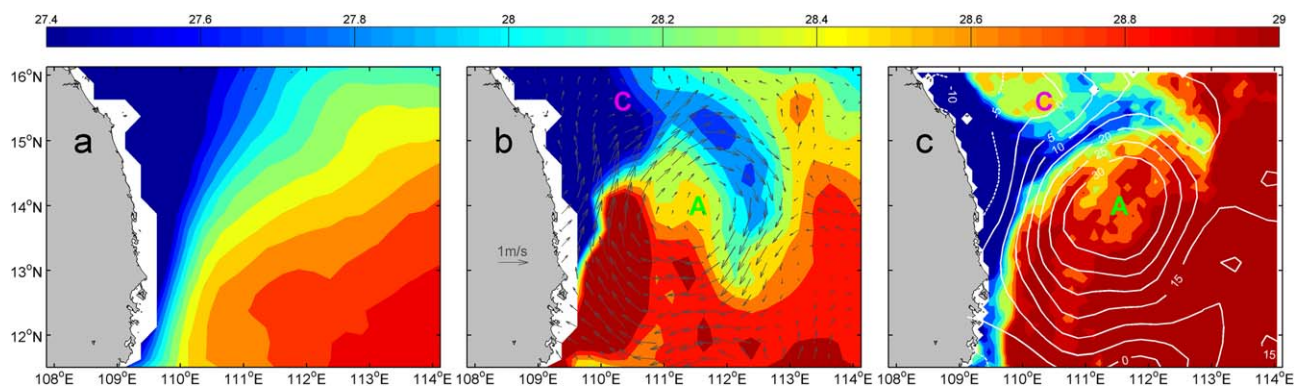


Figure 7. (a) RSS SST (°C) on the grids of AVISO geostrophic currents in April averaged from 2003 to 2013. (b) AVISO geostrophic current anomalies (m/s, vectors) on 3 May 2012 and snapshot SST (°C, color shading) simulated by the mixed layer model. (c) Satellite observed RSS SST (°C, color shading) and SLA (cm, white contours) on 3 May 2012. In Figures 7b and 7c, the anticyclonic (cyclonic) eddy is labeled with A (C).

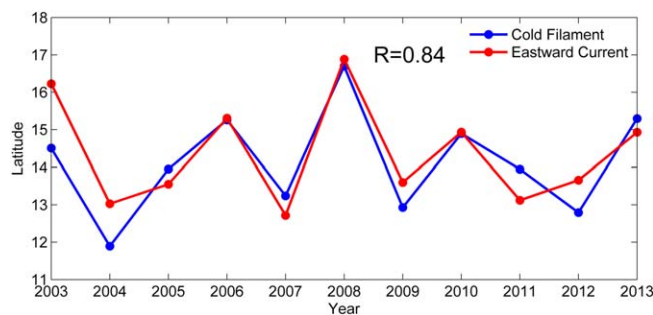


Figure 8. Time series of the mean latitudes of cold filaments and eastward currents from 2003 to 2013.

These cold filaments are found to form frequently in the western coastal boundary of the SCS and extend several hundreds of kilometers offshore, bringing cold and nutrient-rich waters from the western coastal zone into the interior of the SCS. On average, the SST anomalies suggest that the meridional width of cold filament is around 100 km. From the SLA (Figure 6a), the computed geostrophic current in the filament is around 30 cm/s. As a consequence, the estimated volume transport of cold water to the interior of the SCS is around 1.8 Sv assuming a vertical scale of 60 m for a cold filament, which is about 18 times of the average annual discharge of the Pearl River (0.1 Sv).

On interannual time scales, the core location of the cold filament displays considerable meridional shift ranging from 9°N to 18°N. The interannual shift of the cold filament can be attributed to the interannual variability of the location of the eastward current associated with eddies [He et al., 2013]. When the eastward current shifts meridionally, the cold filament shifts in concert, maintaining its connection to the main stream of the eastward current.

Ocean-atmosphere interaction has been found to be very active in regions of cold SSTs [Lin et al., 2003; Chow and Liu, 2012], suggesting that the appearance of spring intermonsoonal cold filaments in the western SCS may have an impact on the atmosphere. Figure 6b shows that the observed wind speed over the cold filament drops on average by 0.5–1.5 m/s relative to that on either side of the filament. Over the cold filament bands, the coefficient of determination between the SST and wind data for the period from 2003 to 2013 reaches 0.4 (Figure 3b). This result suggests that the spring cold SST filaments may have profound effects on the sea surface winds. One possible mechanism is that the cold SST of the filaments cools the bottom of the atmosphere thereby increasing the stability of the atmospheric boundary layer. This, in turn, suppresses the near-surface vertical mixing, which would normally bring stronger wind from aloft toward the lower boundary [Vecchi et al., 2004], and thus reduces the sea surface wind speed. However, to verify and elucidate this mechanism and uncover the detailed air-sea interaction over the cold filaments, a high resolution coupled circulation model including advanced mixed-layer physics would be needed, which is beyond the scope of the present study.

Although the eastward current associated with eddies plays a critical role in the formation and interannual evolution of cold filament in spring, other atmosphere and ocean processes [Xie et al., 2007] may also contribute to their formation and evolution. As shown in Figure 6b, the cold filament also possesses robust intraseasonal variability, which may be associated with the atmospheric intraseasonal wind pulses. Further study is needed to fully understand the source of this variability in the cold filament and the associated dynamic processes controlling it.

Other atmosphere and ocean processes [Xie et al., 2007] may also contribute to their formation and evolution. As shown in Figure 6b, the cold filament also possesses robust intraseasonal variability, which may be associated with the atmospheric intraseasonal wind pulses. Further study is needed to fully understand the source of this variability in the cold filament and the associated dynamic processes controlling it.

Acknowledgments

This study benefited from the RSS SST data (ftp://data.remss.com/SST/daily_v04.0/mw_ir/), wind data of QuickSCAT (<http://data.remss.com/qscat/>) and ASCAT (<ftp://ftp.remss.com/ascatl/>), Chl a concentration data from the MODIS data set (<http://oceancolor.gsfc.nasa.gov/>), SLA data of AVISO (<ftp://ftp.avisioceanobs.com/>), and SCS eddy trajectory data derived from the third release global eddy data set (<http://cioss.coas.oregonstate.edu/eddies/>). This work is supported by the National Basic Research Program of China (2013CB430301), the National Science Foundation of China (91428206, 41125019, 41621064, 91528304), the National Programme on Global Change and Air-Sea Interaction (GASI-IPOVAI-04), and the China Postdoctoral Science Foundation (2016M601493).

References

- Barton, E., M. Inall, T. Sherwin, and R. Torres (2001), Vertical structure, turbulent mixing and fluxes during Lagrangian observations of an upwelling filament system off northwest Iberia, *Prog. Oceanogr.*, *51*, 249–267, doi:10.1016/S0079-6611(01)00069-6.
- Chen, C., and G. Wang (2014), Interannual variability of the eastward current in the western South China Sea associated with the summer Asian monsoon, *J. Geophys. Res. Oceans*, *119*, 5745–5754, doi:10.1002/2014JC010309.
- Chelton, D. B., M. G. Schlax, and R. M. Samelson (2011), Global observations of nonlinear mesoscale eddies, *Prog. Oceanogr.*, *91*(2), 167–216.
- Chow, C. H., and Q. Liu (2012), Eddy effects on sea surface temperature and sea surface wind in the continental slope region of the northern South China Sea, *Geophys. Res. Lett.*, *39*, L02601, doi:10.1029/2011GL050230.
- Cordeiro, N. G. F., R. Nolasco, A. Cordeiro-Pires, E. D. Barton, and J. Dubert (2015), Filaments on the Western Iberian Margin: A modeling study, *J. Geophys. Res. Oceans*, *120*, 5400–5416, doi:10.1002/2014JC010688.
- Ducet, N., P. Y. Le Traon, and G. Reverdin (2000), Global high-resolution mapping of ocean circulation from TOPEX/Poseidon and ERS-1 and -2, *J. Geophys. Res.*, *105*, 19,477–19,498.
- Flament, P., L. Armi, and L. Washburn (1985), The evolving structure of an upwelling filament, *J. Geophys. Res.*, *90*, 11,765–11,778.
- Haynes, R., E. D. Barton, and I. Pilling (1993), Development, persistence and variability of upwelling filaments off the Atlantic coast of the Iberian Peninsula, *J. Geophys. Res.*, *98*, 22,681–22,692.

- He, Z., Y. Zhang, and D. Wang (2013), Spring mesoscale high in the western South China Sea, *Acta Oceanol. Sin.*, 32(6), 1–5, doi:10.1007/s13131-013-0318-0.
- Lin, I.-I., W. T. Liu, C.-C. Wu, J. C. H. Chiang, and C.-H. Sui (2003), Satellite observations of modulation of surface winds by typhoon-induced upper ocean cooling, *Geophys. Res. Lett.*, 30(3), 1131, doi:10.1029/2002GL015674.
- Lin, I.-I., C.-C. Lien, C.-R. Wu, G. T. F. Wong, C.-W. Huang, and T.-L. Chiang (2010), Enhanced primary production in the oligotrophic South China Sea by eddy injection in spring, *Geophys. Res. Lett.*, 37, L16602, doi:10.1029/2010GL043872.
- Liu, W. T., and X. Xie (1999), Space-based observations of the seasonal changes of South Asian monsoons and oceanic response, *Geophys. Res. Lett.*, 26, 1473–1476.
- Lutjeharms, J. R. E., F. A. Shillington, and C. M. Duncombe Rae (1991), Observations of extreme upwelling filaments in the southeast Atlantic Ocean, *Science*, 253, 774–776, doi:10.1126/science.253.5021.774.
- Meunier, T., E. Barton, B. Barreiro, and R. Torres (2012), Upwelling filaments off Cap Blanc: Interaction of the NW African upwelling current and the Cape Verde frontal zone eddy field? *J. Geophys. Res.*, 117, C08031, doi:10.1029/2012JC007905.
- Mooers, C., and A. Robinson (1984), Turbulent jets and eddies in the California Current and inferred cross-shelf transports, *Science*, 223, 51–53.
- Peliz, A., A. M. P. Santos, P. B. Oliveria, and J. Dubert (2004), Extreme cross-shelf transport induced by eddy interactions southwest of Iberia in winter 2001, *Geophys. Res. Lett.*, 31, L08301, doi:10.1016/2004GL019618.
- Qu, T. D. (2001), Role of ocean dynamics in determining the mean seasonal cycle of the South China Sea surface temperature, *J. Geophys. Res.*, 106, 6943–6955.
- Strub, P., P. Kosro, and A. Huyer (1991), The nature of the cold filaments in the California Current System, *J. Geophys. Res.*, 96, 14,743–14,768.
- Sun, R., G. Wang, and C. Chen (2016), The Kuroshio bifurcation associated with islands at the Luzon Strait, *Geophys. Res. Lett.*, 43, 5768–5774, doi:10.1002/2016GL069652.
- Wang, G., J. Li, C. Wang, and Y. Yan (2012), Interactions among the winter monsoon, ocean eddy and ocean thermal front in the South China Sea, *J. Geophys. Res.*, 117, C08002, doi:10.1029/2012JC008007.
- Wang, J., and D. L. Tang (2014), Phytoplankton patchiness during spring intermonsoon in western coast of South China Sea, *Deep Sea Res., Part II*, 101, 120–128.
- Washburn, L., M. Swenson, J. Largier, P. Kosro, and S. Ramp (1993), Cross-shelf sediment transport by an anticyclonic eddy off Northern California, *Science*, 261, 1560–1564.
- Xie, S.-P., Q. Xie, D. Wang, and W. Liu (2003), Summer upwelling in the South China Sea and its role in regional climate variations, *J. Geophys. Res.*, 108(C8), 3261, doi:10.1029/2003JC001867.
- Xie, S.-P., C.-H. Chang, Q. Xie, and D. Wang (2007), Intraseasonal variability in the summer South China Sea: Wind jet, cold filament, and recirculations, *J. Geophys. Res.*, 112, C10008, doi:10.1029/2007JC004238.
- Vecchi, G., S.-P. Xie, and A. Fischer (2004), Ocean-atmosphere covariability in the western Araian Sea, *J. Clim.*, 17, 1213–1224.

Erratum

In the originally published version of this article, there was an error in the funding information in the Acknowledgments. “Natural Science Foundation of China (41406004)” has been changed to “Natural Science Foundation of China (41125019),” and this version may be considered the authoritative version of record.